CHEMISTRY OF MATERIALS
Article

Chem. Mater. **2010,** *22,* 5137–5153 5137
DOI:10.1021/cm101755j

Calcium Phosphate−Gelatin Nanocomposites: Bulk Preparation (Shape- and Phase-Control), Characterization, and Application as Dentine Repair Material

Theresa Kollmann,[†] Paul Simon,[†] Wilder Carrillo-Cabrera,[†] Carola Braunbarth,[‡] Tilo Poth,[‡] Elena V. Rosseeva,[†] and Rüdiger Kniep*[,†]

[†]*Max-Planck-Institut für Chemische Physik fester Stoffe, Nöthnitzer Strasse 40, 01187 Dresden, Germany, and* [‡]*SusTech GmbH & Co. KG Darmstadt, Petersenstrasse 20, 64287 Darmstadt, Germany*

Received June 23, 2010. Revised Manuscript Received July 26, 2010

Nanocomposites consisting of gelatin and hydroxyapatite as well as of gelatin and mixtures of hydroxyapatite and different amounts of octacalcium phosphate were prepared as bulk-materials. The composites were precipitated from aqueous solutions of $CaCl_2 \cdot 2H_2O$ and $(NH_4)_2(HPO_4)$, respectively, with varying amounts of gelatin at 25 °C and pH 7. The influence of prestructuring effects of calcium and phosphate ions, respectively, on gelatin and by this on the precipitated materials was investigated in detail. X-ray-diffraction (XRD), energy dispersive X-ray spectroscopy (EDXS), and high-resolution transmission electron microscopy (HR-TEM) revealed that the prestructuring components as well as the total amount of gelatin involved in the reactions have a substantial influence on the composition and shape of the nanocomposites formed. In the case of $CaCl_2 \cdot 2H_2O$ used as the prestructuring agent for gelatin, hydroxyapatite is the inorganic phase obtained, independent of the initial amount of gelatin. By the prestructuring of gelatin with $(NH_4)_2(HPO_4)$, a strong dependency of the reaction products on the amount of gelatin was observed. Low gelatin quantities favor the formation of hydroxyapatite, whereas high gelatin concentrations lead to the formation of octacalcium phosphate. Moreover, the morphology of the composites changes gradually. Samples prepared by means of the Ca-prestructuring (CPS) reaction consist of small plate-like particles (∼50 nm × 33 nm). When the PO_4-prestructuring (PPS) reaction is used, the particle size is highly influenced by the amount of gelatin. Lower gelatin concentrations lead to small, plate-like particles (∼60 nm × 35 nm), while higher gelatin concentrations cause the development of large foils (∼730 nm × 410 nm). The thickness of the composite particles varies from 2 to 13 nm as determined by means of electron holography. The calcium phosphate−gelatin nanocomposites obtained by the precipitation reactions were investigated for use as dentine repair materials with a special focus on the closing of open tubuli of sensitive tooth necks.

Introduction

Hard tissues such as bone and teeth are composed of calcium phosphate in the form of hydroxyapatite (HAP, $Ca_{10}(PO_4)_6(OH)_2$), together with a large number of proteins as organic components.[1] Bone and tooth dentine contain collagen as the organic matrix (∼25−40 wt % and ∼20−30 wt %, respectively), while tooth enamel contains amelogenins and enamelins (∼0.1−4.0 wt %).[1−7] Functional groups which are present on the surface of the matrix molecules serve as nucleation sites and lead to self-assembly phenomena and to the formation of the biominerals.[1,8] Octacalcium phosphate (OCP, $Ca_8(HPO_4)_2(PO_4)_4 \cdot 5H_2O$) and amorphous calcium phosphate (ACP) were proposed to act as precursor phases during the formation of biological HAP.[9−11] By means of transmission electron microscopy (TEM), it was shown that enamel and dentine crystallites exhibit a dark line of 1−1.5 nm width along their centers, the so-called central dark line (CDL). The CDL has been attributed to the presence of planar defects such as dislocations and grain boundaries,[12,13] and more recently to the presence of a layer of OCP within dentine

*Corresponding author. Tel: +49-351-46 46 30 00. Fax: +49-351-46 46 30 02. E-mail: kniep@cpfs.mpg.de..

(1) Mann, S. *Biomineralization: Principles and Concepts in Bioorganic Materials Chemistry*; Oxford University Press, New York, 2001.
(2) Dorozhkin, S. V.; Epple, M. *Angew. Chem., Int. Ed.* **2002**, *114*, 3260.
(3) Elliott, J. C. *Structure and Chemistry of the Apatites and Other Calcium Orthophosphates*; Elsevier: Amsterdam, 1994.
(4) Elliott, J. C. *Rev. Miner. Geochem.* **2002**, *48*, 427.
(5) Gross, K. A.; Berndt, C. C. *Rev. Miner. Geochem.* **2002**, *48*, 631.
(6) Frank-Kamenetskaya, O. V.; Golubtsov, V. V.; Pikhur, O. L.; Zorina, M. L.; Plotkina, Yu. V. *Proc. Russ. Mineral. Soc.* (*Zapiski RMO*) **2004**, *5*, 104.
(7) Ferdinand, C. M.; Driessens, R. M.; Verbeeck, H. *Biominerals*; CRC Press: Boca Raton, FL, 1990.
(8) Mann, S. *Nature* **1988**, *332*, 119.
(9) Brown, W. E.; Eidelmann, N.; Tomazic, B. *Adv. Dent. Res.* **1987**, *1*, 306.
(10) Posner, A. S.; Betts, F. *Acc. Chem. Res.* **1975**, *8*, 273.
(11) Posner, A. S. *J. Dent. Res.* **1997**, *76*(8), 1433.
(12) Bres, E. F.; Hultchison, J. L.; Voegel, J.-C.; Frank, R. M. *J. Phys.* (*Paris*) **1990**, *51*, 97.
(13) Bres, E. F.; Waddington, W. G.; Voegel, J.-C.; Barry, J. C.; Frank, R. M. *Biophys. J.* **1986**, *50*, 1185.

Published on Web 08/11/2010

and enamel crystallites.[14−16] However, it is still one of the controversial issues in the biomineralization of teeth whether enamel and dentine apatite are formed directly or via intermediate metastable phases.

Many research groups have been trying to develop an artificial calcium phosphate biomaterial for hard tissue repair using biomimetic processes.[17,18] Thereby, precipitation reactions and double diffusion techniques were widely used. Collagen, as the natural organic matrix in dentine and bone, is often replaced by its denaturated form (gelatin), because of lower costs, commercial availability, solubility in aqueous systems, and the well-defined physical and chemical properties.[19] Several years ago, Chang et al. first used the coprecipitation method with gelatin as an artificial biomimetic procedure.[19,20] It was observed that the crystallite size decreased with increasing initial amount of gelatin. This observation was explained by a heterogeneous nucleation reaction: Ca^{2+} ions bind to the carbonyl groups of gelatin, and afterward, phosphate ions are attached at these calcium positions. The higher the number of nucleation sites that exist, the more tiny HAP crystallites can be formed. In this connection, also the influence of some modifier molecules such as glutaraldehyde and polyvinylalcohol on the HAP−gelatin system was studied.[21,22] Other groups examined the influence of additives such as alginate and doping with magnesium.[23,24] Instead of coprecipitation reactions, also titration methods have been used in which Ca^{2+} ions act as prestructuring components for the preparation of HAP−gelatin nanocomposites.[25,26] Furthermore, the influence of external electrical fields[27] as well as the influence of water-in-oil emulsions using gelatin droplets as microreactors have been investigated.[28] Recently, Landfester et al. prepared gelatin nanoparticles in inverse miniemulsions, providing a spatial confinement during HAP-composite precipitation.[17] Chen et al. reported on the preparation of gelatin coated HAP nanoparticles.[29] In the case of these investigatons, needle-, rod-, or fibril-like morphologies of the particles were preferably obtained.[20−24,28,29]

Besides precipitation reactions, double diffusion techniques represent another approach to mimic a biogenic system with respect to calcium phosphate mineralization.[30−44] Fluorapatite−gelatin nanocomposites were grown in gelatin gel matrixes by double diffusion experiments.[32] These investigations revealed that two different growth mechanisms appear within this system: the so-called fractal and the fan-like growth mechanisms. The fractal growth mechanism preferentially occurs in the PO_4-prestructured areas of the gel,[32] whereas the fan-like growth mechanism dominates in the Ca-prestructured regions.[40] Their main differences in morphology can be summarized as follows: aggregates of the fractal growth mechanism reveal bent and rounded morphologies, whereas aggregates of the fan-like growth mechanism are of a more straight and cornered habit. The experimental observations were supported by atomistic computer simulations.[40,44] The gelatin molecules were simulated as a model of three twisted (glycine−proline−4-hyroxyproline)$_{12}$ polypeptide strands. It was found that the binding positions strongly depend on the ionic species. Calcium ions preferably bind to the carbonyl-oxygen atoms of the polypeptide backbone and to oxygen atoms of hydroxyproline residues. Even though calcium association causes the opening of some hydrogen bonds between the peptide strands, no remarkable configurational changes of the straight triple-helical molecules occur. Rather, the rigidity of the molecule is increased by fixation of calcium ions inside the polypeptide strands. The situation changes completely in the case of phosphate association. Phosphate ions are preferably attached outside the triple-helix, forming two to three hydrogen bonds with hydroxyproline side groups and partially also with the amino groups. Depending on the amount of hydrogen bonds formed, the gelatin molecule undergoes a strong deformation. The triple-helix becomes more and

(14) Bres, E. F.; J, C.; Barry, J. C.; Hultchison, J. L. *Ultramicroscopy* **1984**, *12*, 367.
(15) Bodier-Houlle, P.; Steuer, P.; Voegel, J. C.; Cuisinier, F. J. G. *Acta Crystallogr., Sect. D* **1998**, *54*, 1377.
(16) Robinson, C.; Connell, S.; Kirkham, J.; Shore, R.; Smith, A. *J. Mater. Chem.* **2004**, *14*, 2242.
(17) Ethirajan, A.; Ziener, U.; Chuvilin, A.; Kaiser, U.; Cölfen, H.; Landfester, K. *Adv. Funct. Mater.* **2008**, *18*, 2221–2227.
(18) Meyer-Lueckel, H.; Cölfen, H.; Verch, A.; Tschoppe, P. *Caries Res.* **2010**, *44*, 127.
(19) Chang, M. C.; Ko, C. C.; Douglas, W. H. *Biomaterials* **2003**, *24*, 2853.
(20) Chang, M. C.; Douglas, W. H.; Tanaka, J. *J. Mater. Sci: Mater. Med.* **2006**, *17*, 387.
(21) Chang, M. C.; Ko, C. C.; Douglas, W. H. *Biomaterials* **2003**, *24*, 3087.
(22) Chang, M. C. *J. Mater. Sci.* **2005**, *40*, 505.
(23) Teng, S.; Shi, J.; Peng, B.; Chen, L. *Compos. Sci. Technol.* **2006**, *66*, 1532.
(24) Yang, Z.; Jiang, Y.; Yu, L. X.; Wen, B.; Li, F.; Sun, S.; Hou, T. *J. Mater. Chem.* **2005**, *15*, 1807.
(25) Kim, H. W.; Knowles, J. C.; Kim, H. E. *J. Biomed. Mater. Res., Part B* **2005**, *74B*, 686.
(26) Fomin, A. S.; Barinov, S. M.; Ievlev, V. M.; Fadeeva, I. V.; Komlev, V. S.; Belonogov, E. K.; Turaeva, T. L. *Dokl. Chem.* **2006**, *411*, 219.
(27) Tanka, S.; Shiba, N.; Senna, M. *Sci. Technol. Adv. Mater.* **2006**, *7*, 226.
(28) Teng, S; Chen, L.; Guo, Y; Shi, J. *J. Inorg. Biochem.* **2007**, *101*, 686.
(29) Chen, M.; Tan, J.; Lian, Y.; Liu, D. *Appl. Surf. Sci.* **2008**, *254*, 2730.
(30) Falini, G.; Gazzano, M.; Ripamonti, A. *J. Mater. Chem.* **2000**, *10*, 535.
(31) Teng, S.; Shi, J.; Chen, L. *Colloids Surf., B* **2006**, *49*, 87.
(32) Kniep, R.; Busch, S. *Angew. Chem.* **1996**, *108*, 2787.Angew. Chem., Int. Ed. Engl. **1996**, *35*, 2624.
(33) Busch, S.; Dolhaine, H.; DuChesne, A.; Heinz, S.; Hochrein, O.; Laeri, F.; Podebrand, O.; Vietze, U.; Weiland, T.; Kniep, R. *Europ. J. Inorg. Chem.* **1999**, *10*, 1643.
(34) Busch, S.; Schwarz, U.; Kniep, R. *Chem. Mater.* **2001**, *13*, 3260.
(35) Busch, S.; Schwarz, U.; Kniep, R. *Adv. Funct. Mater.* **2003**, *13*, 189.
(36) Simon, P.; Carrillo-Cabrera, W.; Formanek, P.; Göbel, C.; Geiger, D.; Ramlau, R.; Tlatlik, H.; Buder, J.; Kniep, R. *J. Mater. Chem.* **2004**, *14*, 2218.
(37) Göbel, C.; Simon, P.; Buder, J.; Tlatlik, H.; Kniep, R. *J. Mater. Chem.* **2004**, *14*, 2225.
(38) Simon, P.; Schwarz, U.; Kniep, R. *J. Mater. Chem.* **2005**, *15*, 4992.
(39) Simon, P.; Zahn, D.; Lichte, H.; Kniep, R. *Angew. Chem., Int. Ed.* **2006**, *118*, 1945. *Angew. Chem., Int. Ed.* **2006**, *45*, 1911.
(40) Tlatlik, H.; Simon, P.; Kawska, A.; Zahn, D.; Kniep, R. *Angew. Chem., Int. Ed.* **2006**, *118*, 1939. *Angew. Chem., Int. Ed.* **2006**, *45*, 1905.
(41) Kniep, R.; Simon, P. *Topics in Current Chemistry: Biomineralization I*; Springer: Heidelberg, Germany, 2007; Vol. *270*, p 73.
(42) Kniep, R.; Simon, P. *Angew. Chem., Int. Ed.* **2008**, *47*, 405.
(43) Rosseeva, E.; Buder, J.; Simon, P.; Frank-Kamenteskaya, O.; Kniep, R. *Chem. Mater.* **2008**, *20*, 6003.
(44) Kawska, A.; Hochrein, O.; Brickmann, J.; Kniep, R.; Zahn, D. *Angew. Chem., Int. Ed.* **2008**, *47*, 4982.

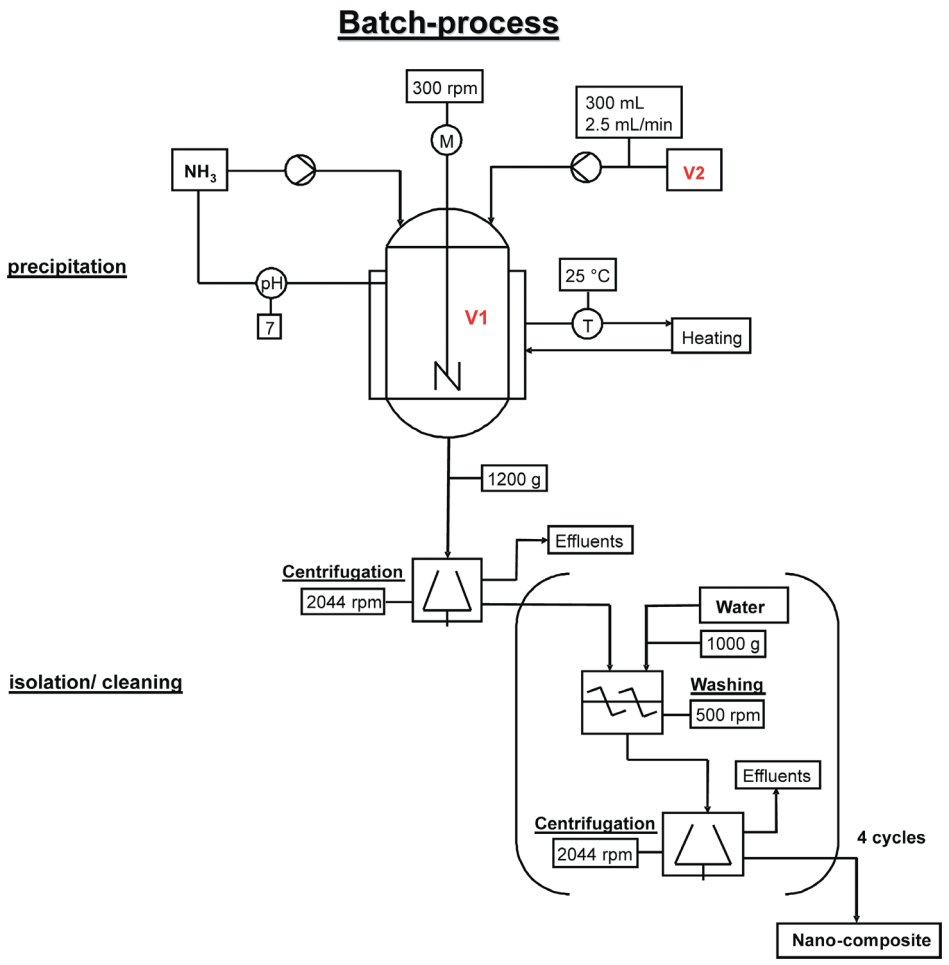

Figure 1. Experimental setup for the precipitation reactions. The preparation procedure includes the two parts precipitation and isolation/cleaning. For further details see text. Ca-prestructuring (CPS) reaction: V1 = aqueous $CaCl_2 \cdot 2H_2O$/gelatin-mixture; V2 = aqueous $(NH_4)_2HPO_4$-solution. PO_4-prestructuring (PPS) reaction: V1 = aqueous $(NH_4)_2HPO_4$/gelatin-mixture; V2 = aqueous $CaCl_2 \cdot H_2O$-solution.

more bent, a situation which can be traced back by the attachment of further phosphate groups at other positions of the macromolecule. Altogether, the gelatin triple-helix keeps its flexibility.

Considering the results of the atomistic simulations and the double diffusion experiments, we tried to apply the observation rigid vs flexible to a precipitation reaction. Precipitation methods have two significant advantages compared with the double diffusion route. First of all, large amounts of reaction products can be produced within a short period of time and with constant material properties. Second, fast precipitation generates a high concentration of nucleation centers, which finally leads to nanosized materials with high specific surface area and, hence, a significant reactivity.

Here, we present a precipitation strategy including the variation of prestructuring (PS) effects in order to control rigidity and/or flexibility of the gelatin precursor. PS effects as well as the amount of gelatin provided during the precipitation reactions influence the shape (size and thickness) and the inorganic phase (HAP or mixtures of OCP and HAP) of the composite materials. Finally, the suitability of the composites for use as dentine repair material is described in detail.

Experimental Section

Preparation. *Precipitation Reaction.* Calcium phosphate−gelatin nanocomposites were prepared by precipitation from aqueous solutions. $CaCl_2 \cdot 2H_2O$ (p. a., Merck, Darmstadt, Germany), $(NH_4)_2(HPO_4)$ (p. a., Riedel-de Haen, Seelze, Germany), and gelatin (300 bloom, acid bovine bone, technical, DGF Stoess AG, Eberbach, Germany) were used as starting reagents. A final Ca/P ratio of 1.67 was kept for all of the reactions by using 0.300 mol $CaCl_2 \cdot 2H_2O$, 0.180 mol $(NH_4)_2HPO_4$, and a total reaction volume of 2.3 L. The amount of gelatin was chosen as 0 g, 9 g, 30 g, and 50 g, respectively. During precipitation, the temperature was kept constant at 25 °C, and the pH was controlled to be 7.0 ± 0.1 by using an aqueous ammonia solution. Stirring was applied at 300 rpm. The experimental setup consisted of a 3 L cylindrical glass reactor, a 3-fold impeller, a heating and a circulating bath, two slope pumps, a pH-controller, and a stirring motor as shown in Figure 1. In order to study the prestructuring effects, two different kinds of reaction procedures were carried out: the calcium prestructuring reaction and the phosphate prestructuring reaction.

Ca Prestructuring (CPS) Reaction. Two solutions were prepared: a gelatin solution at 50 °C and a Ca-recipient solution at ambient temperature. The solutions were filled into the reaction vessel under mild stirring. The pH-value of the system was adjusted to 7.0 ± 0.1 by using HCl(aq). Three hundred milliliters of a neutralized 0.6 M $(NH_4)_2HPO_4$ aqueous solution was dropped into the reaction mixture at a rate of 2.5 mL/min.

During the entire precipitation process, stirring at 300 rpm was applied. The pH value was controlled at 7.0 ± 0.1, and the temperature was held at 25 °C. After two hours of precipitation, the milky suspension was left under constant conditions (25 °C, pH 7, 300 rpm) for 21 h. In order to isolate and clean the resulting precipitate, 1200 g of the aged suspension was centrifuged at 2044 rpm for 15 min, suspended again in 1000 g of deionized water, and washed by stirring at 500 rpm for 10 min to remove salts and excessive gelatin. Four cycles of washing and centrifugation were required. Finally, a small portion of the white precipitate was suspended in ethanol for investigation by transmission electron microscopy. The rest was frozen by liquid nitrogen and dried in a freeze-drier for preservation.

PO_4 Prestructuring (PPS) Reaction. The entire procedure was performed by using $(NH_4)_2HPO_4$ as the prestructuring reagent. The gelatin solution was prepared at 50 °C, and the phosphate recipient solution was prepared at ambient temperature. Both solutions were filled into the glass reactor and the pH-value was adjusted to 7.0 ± 0.1 with NH_3(aq). The precipitation was performed with 300 mL of a neutralized 1.0 M $CaCl_2 \cdot 2H_2O$ aqueous solution. The dropping rate of the precipitation reagent, the temperature, the pH value, the stirring rate, and the ripening time as well as the way of isolation/cleaning stayed the same as described for the Ca prestructuring reaction.

Samples Coding. In the following, the samples are coded according to the prestructuring ion and to the amount of gelatin used for the reactions. In the case of the CPS reaction, samples were labeled with a C and in the case of PPS reactions with a P. The initial amount of gelatin is attached as G with the corresponding quantity. For example, the CPS reaction with 30 g of gelatin is coded as C-G30.

Dentine Slab Preparation for SEM Investigations. Roots of bovine incisors were cut lengthwise by a diamond saw (Clipper 202, Norton Clipper, Stephenville, USA). Subsequently, the two halves were additionally cut laterally (once or twice). Thus, every root yielded four to six samples (~ 1 cm × 1 cm × 0.5 cm) depending on its original size. Every sample was fixed by a thermoplastic glue on a Plexiglas specimen holder, mounted in a grinder (RotoPol 31 with RotoForce 4, Struers, Willich, Germany), and ground with a diamond grinding disk of 10 μm grain size, as long as the enamel was removed. Then, the grinding disk was replaced by a polishing disk (MD-Nap, Struers, Willich, Germany). A colloidal diamond suspension (DP Diamantsuspension M, grain size 1 μm, Struers, Willich, Germany) was used as the polishing medium (polishing time: 2 min). Between these two steps as well as after polishing, the dentine slabs were cleaned in an ultrasonic bath. Finally, the slabs were dried in warm air flow and checked by means of environmental scanning electron microscopy (ESEM) according to their specific characteristics (positions and opening degrees of the tubules).

Preparation of Artificial Saliva Solution (AS)[45]. The artificial saliva solution was prepared in a 5.0 L volumetric flask and contained 1.5 mM $CaCl_2$, 0.9 mM KH_2PO_4, 130 mM KCl, and 20 mM Hepes buffer (Roth). The pH was adjusted to 7.0 by 2 M NaOH.

Treatement of Dentine Slabs with Dispersions of the Composite (P-G30) in Water/Glycerine. Fifteen grams of a 2 wt % dispersion of the composite material P-G30 in a water/glycerine (1:3) mixture was prepared. The slurry was stirred at 400 rpm for 15 min at 25 °C. This dipping solution was renewed every second or third day. Between the dips, the slurry was stored at 4 °C. Before performing the dips, the slurry was stirred again at 400 rpm for 15 min at 25 °C. Before the first treatment, the dentine slab had to be cleaned. For this, it was converted into a test tube filled with 1.5 wt % Empicol-solution, ultrasonically treated for 5 min, and subsequently rinsed with AS. The dentine slab treatment was carried out over a period of 10 days with once daily brushing (in the "morning") and twice daily dipping (once in the "morning" and once in the "afternoon") in the 2 wt % dispersion with subsequent storage in AS. Every "morning", the dentine slab was rinsed with AS, fixed in an especially prepared brushing device, covered with several drops of a water/glycerine (1:1) mixture, and brushed for 1 min by means of a conventional rotation tooth brush mounted in the brushing device (contact pressure: 150 g). After brushing, the dentine slab was rinsed with AS and immediately placed in the 2 wt % dipping dispersion for 10 min. After exactly 10 min, the slab was removed, converted into the vessel containing 20 mL of fresh AS, and stored at 37 °C (water bath) until the next treatment in the "afternoon" was started. In the "afternoon", the dentine slab was rinsed with AS, dipped again in the 2 wt % dispersion for 10 min, and stored until the next "morning" in 20 mL of fresh AS at 37 °C. After 10 days, the dentine slab was rinsed with AS after the last dip and stored under dry conditions for ESEM investigations.

Treatment of a Dentine Slab with Composite Dispersion (C-G30) in a Conventional Tooth Paste (Theramed, Henkel KGaA). A conventional tooth paste containing 1450 ppm fluoride (NaF) was used as basic material after adding a 1 wt % dispersion of C-G30. Before treatment of the dentine slab, the dispersion was additionally mixed with water in the ratio of 1:1 and stirred at 400 rpm at 25 °C for 15 min. Between the brushing treatments in the "morning" and in the "afternoon", the slurry was stirred at 400 rpm at 25 °C. The slurry was renewed every day. Before the first brushing, the dentine slab was cleaned with a 1.5 wt % Empicol-solution and ultrasonic treatment for 5 min, followed by subsequent rinsing with AS. The whole process of the dentine slab treatment took a period of 10 days with twice a day brushing (once in the "morning" and once in the "afternoon"), in each case for 1 min. The brushing device used was the same as that described above. After brushing, the dentine slab was subsequently converted into a vessel containing 20 mL of fresh AS and stored at 37 °C (water bath) until the next brushing procedure was started. After the entire treatment over 10 days, the dentine slab received a final 1 min brushing with a 1:1 water/glycerine mixture and a final rinse with water. The slab was stored under dry conditions for ESEM investigations.

FIB Preparation of Dentine Slabs for TEM Investigation. A dentine slab, obtained by means of brushing treatments with a dispersion of 1 wt % C-G30 in a conventional tooth paste was cut into thin longitudinal slices of about 100 μm thickness by the use of a wire saw (type ws 22, K. D. UNIPRESS, Warszawa, Poland) containing a tungsten wire (50 μm) lubricated with boron carbide suspended in glycerine (86 wt % aqueous solution). The final size of the slice was laterally reduced to 1 mm−2 mm in order to fit the TEM holder (3 mm half ring). For the preparation of FIB sections, a thin lamella of about 100 nm−200 nm thickness was cut from this slice. The window size (corresponding to length of the lamella) amounted to about 8 μm. In order to release the stress from the thin lamella, both sides of the lamella (laterally left and right) were separated from the bulk sample.

Treatment of the Composite for the Inner Structure Investigations. Partial dissolution of the inorganic part of the composite

(45) ten Cate, J. M.; Buijs, M. J.; Damen, J. J. M. *Eur. J. Oral. Sci.* **1995**, *103*, 362.

was performed by dipping the sample prepared on a TEM-grid in a 0.2N aqueous EDTA-solution for 5 s. The process was stopped by rinsing with water. Additional staining was performed by dipping the "loaded" TEM-grid in a 0.5 wt % aqueous UAc-solution for 30 s. Finally, the TEM-grid was rinsed with water again and carefully dried.

Characterization. *Chemical Analysis*. Calcium and phosphorus were analyzed by EDXS. The amount of gelatin within the composite was determined indirectly by taking the nitrogen content of pure gelatin as a standard. The nitrogen contents of the composite as well as of pure gelatin were determined by the carrier-gas hot-extraction method combined with a combustion technique (CHNS-analyzer 932, LECO, St. Joseph, Michigan, USA). For the measurements, 2 mg of each sample was combusted in a Sn capsule under O_2-atmosphere.

FT-IR Spectroscopy. Fourier transform infrared (FT-IR) spectra in the region of 4000−400 cm^{-1} were recorded at ambient temperature using a Bruker spectrometer (IFS 66v/S; Globar (MIR), KBr, DTGS-Detector; Program Opus/IR 3.0.3). The samples were prepared as KBr pellets (1 mg of the material under investigation dispersed in 150 mg of KBr).

X-ray Diffraction (*XRD*). The crystalline inorganic components of the composites were determined by powder X-ray diffraction. The samples were ground in an agate mortar and then fixed with vaseline glue between two Kapton-foils (0.1 mm). The powder patterns were collected on a Guinier Imaging Plate Camera HUBER G670 (Cr$K_{\alpha 1}$-radiation, $\lambda = 2.28970$ Å, germanium (111) monochromator). The measurement time was 10 × 30 min in the range of $4.0° < 2\theta < 100.0°$. In order to exclude misinterpretation of the XRD patterns (interference of reflections from calcium phosphate phases by vaseline glue), the effect of vaseline glue on the diffraction patterns was investigated in more detail. Data analysis and phase identification were carried out by means of the program packages WinXPow[46] and WinCSD.[47] The size of the coherence scattering domains (CSD) of the apatite crystallites along their *c*- and *a*-axes were calculated from the Scherrer equation[48] using the (002) and (300) reflections, respectively. Cr$K_{\alpha 1}$-radiation was used in order to achieve a better resolution of reflections at low 2θ angles, which is especially needed for identification of the strongest and most characteristic (100)-reflection of OCP.[49]

Transmission Electron Microscopy (*TEM*). Morphology (size and thickness) and crystal phase of the composites were either investigated by using a CM 200 ST-Lorentz electron microscope (FEI, Eindhoven, Netherlands) with FEG-source at an accelerating voltage of 200 keV or by a FEI Tecnai 10 electron microscope (FEI company, Eindhoven, Netherlands) with a LaB_6-source at 100 kV acceleration voltage. For sample preparation, a small amount (spatula tip) of the as-prepared precipitate was diluted in about 10 mL of ethanol. A drop of this suspension was placed on a TEM-grid (holey carbon film on 300 mesh Cu-grid, Plano GmbH, Wetzlar, Germany) which was plasma-etched for 10 s (Plasma Prep II, SPI Supplies, West Chester, USA). Plasma-etching was performed to flatten the foil-like particles. For TEM investigations of the dentine slabs, focused ion beam (FIB) thin cuts were prepared by the use of an FEI Quanta 200 3D dual beam device (FEI, Eindhoven, Netherlands). Subsequently, the TEM measurements were performed with the same microscopes as that given above.

Electron Holography. Particle thicknesses were determined by means of electron holography. As in conventional TEM, in holography electrons are also treated as waves according to de Broglie: $\lambda = h/(mv)$. Therefore, the interaction between the incident electron beam and the sample (matter) can be described as a plane wave with a certain amplitude (a) which experiences a certain phase shift ($\Delta\varphi$). The phase shift ($\Delta\varphi$) is proportional to the product of the mean inner potential (U_i) of the sample and its thickness (d) along the incident beam:

$$\Delta\varphi = C_E U_i d \quad (1)$$

where C_E is the interaction parameter [V^{-1} nm^{-1}].

The microscope was used at an acceleration voltage of 200 kV; C_E amounts to 0.0073 V^{-1} nm^{-1} at a wavelength of $\lambda = 2.5$ pm. In holography, both, the amplitude (a) and the phase (φ) of the image are given by the amplitude and the phase transfer function. The holography setup can be described as follows: The illuminating wave is divided into an object wave and a reference wave. The object wave which penetrates the sample is affected in amplitude and phase. The reference wave goes through a vacuum and is therefore not affected. Subsequently, the object and the reference waves are superimposed by an electron biprism. The resulting interference image, the so-called hologram, is given by the following:

$$I_{hol}(x) = 1 + a^2(x) + 2a(x)\cos[2\pi q_c x + \varphi(x)] \quad (2)$$

where q_c is the spatial frequency of the interference fringes, and I_{hol} is the intensity.

The electron biprism consists of a positively charged wire between the object lens and the first intermediate image. The resulting hologram is recorded by a CCD camera. By means of computer-based numerical image processing (FT), the recorded wave can be separately reconstructed in amplitude (a) and phase (φ). In general, a field emission gun with a monochromatic and coherent illumination is implicitly necessary to obtain a high contrast of the hologram fringes.

For thickness determinations, flat laying particles (free-standing, isolated plates or foils separated from the agglomerates) were used. According to eq. 1, the thickness (d) can be calculated from the phase shift ($\Delta\varphi$), the inner potential (U_i), and the interaction parameter (C_E).

Scanning Electron Microscopy (*SEM*) *and Energy Dispersive X-ray Spectroscopy* (*EDXS*). Investigations were carried out by means of an ESEM FEI Quanta 200 FEGi system in high vacuum mode and at an acceleration voltage of 15 kV (FEI, Eindhoven, Netherlands). For EDXS measurements, the device was additionally equipped with the system Genesis 2000 (EDAX, AMETEK, Wiesbaden, Germany). Samples were powdered in an agate mortar. The powder was fixed on a double-bonding carbon pad, which was placed on an alumina or brass support. Finally, the samples were sputtered with gold for 30 s.

Results and Discussion

Phase Composition and Coherence Scattering Domains (CSD). The XRD patterns of samples precipitated by the CPS reaction and gelatin amounts of 0 g, 9 g, 30 g, and 50 g (C-G0, C-G9, C-G30, and C-G50) are presented in Figure 2 (in addition, the calculated powder pattern of

(46) WinXPow 2.22; STOE & Cie GmbH: Darmstadt, Germany, 2005.
(47) Akselrud, L. G.; Zavalii, P. Y.; Grin, Y. N.; Pecharsky, V. K.; Baumgartner, B.; Wölfel, E Use of CSD program package for structure determination from powder data. *Mater. Sci. Forum* **1993**, *133−136*, 335.
(48) Scherrer, P. *Göttinger Nachrichten Gesell.* **1918**, *2*, 98.
(49) Brown, W. E. *Nature* **1962**, *196*, 1048.

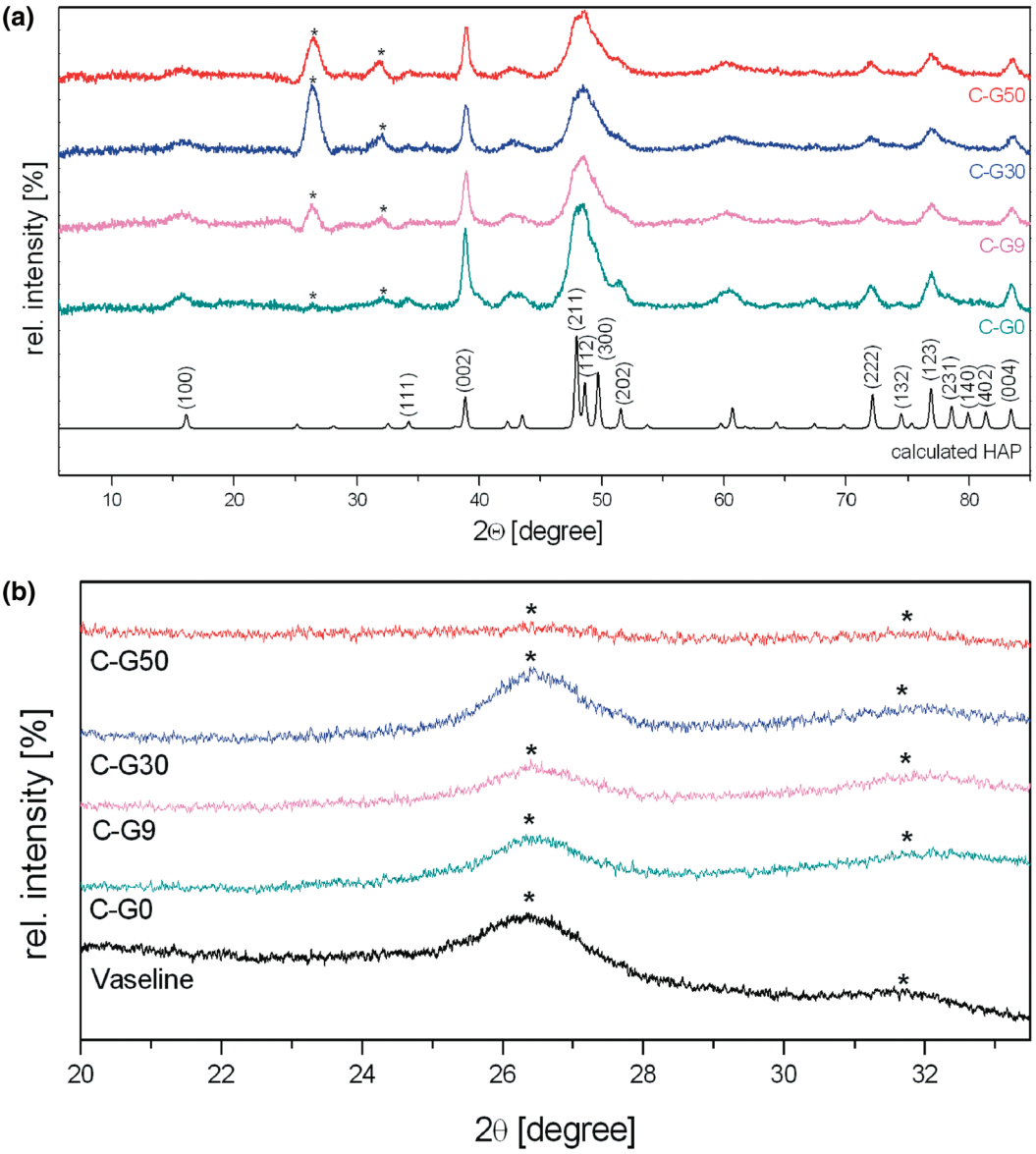

Figure 2. (a) XRD patterns ($CrK_{\alpha 1}$) of samples precipitated by the CPS reaction and gelatin amounts of 0 g, 9 g, 30 g, and 50 g (C-G0, C-G9, C-G30, and C-G50) together with the calculated powder pattern of HAP.[50] Peaks marked with an asterisk belong to vaseline used as glue in the XRD preparation as well as to poorly crystalline or amorphous phases, such as ACP[51] or some transition states between calcium phosphate phases. For further details, see the text. (b) Cutout between $20° < 2\theta < 33.5°$ of XRD patterns ($CrK_{\alpha 1}$) of pure vaseline and samples precipitated by the CPS reaction with gelatin amounts of 0 g, 9 g, 30 g, and 50 g (C-G0, C-G9, C-G30, and C-G50) prepared without vaseline as glue. Reflections marked with an asterisk indicate that they belong to poorly crystalline HAP or even ACP and not only to vaseline.

HAP[50] is shown). Most of the diffraction peaks observed in the XRD patterns of the reaction products correspond to HAP. The majority of the peaks are broad and weak, indicating that the inorganic phase is only poorly crystalline. The relative intensities of (002) and (004) reflections, however, are remarkable strong. The same effect is observed for the (112)-reflection, which is of similar intensity compared with that of the (211)-reflection and also for all the reflections in the 2θ-region between 70° and 85°. Thus, only reflections with large *c*-axis components are observed. This also suggests a highly preferred orientation (texture effect) and/or elongation of HAP nanosubunits along [001]. As illustrated in Figure 2a, the relative intensities of the major HAP diffraction peaks decrease with increasing gelatin content, while the peak-width is increased. At the same time, the relative intensities of the reflections at 2θ around 26° and 32° increase (peaks marked with an asterisk), indicating an increasing content of only poor crystallinity, or amorphous phases, such as amorphous calcium phosphate (ACP),[51] or some transitions between calcium phosphate phases. In previous investigations, it was demonstrated that ACP has an apatitic short-range order showing an XRD pattern considered as typical for ACP.[51] In particular, it was illustrated that in the XRD pattern of ACP the relative intensity of some reflections is significantly higher compared with respective reflections in the XRD pattern of HAP. Figure 2b illustrates cutouts of

(50) Kay, M. I.; Young, R. A.; Posner, A. S. *Nature* **1964**, *204*, 1059.

(51) Hu, Q.; Tan, Z.; Liu, Y.; Tao, J.; Cai, Y.; Zhang, M.; Pan, H.; Xu, X.; Tang, R. *J. Mater. Chem.* **2007**, *17*, 4690.

Table 1. Variation of the Size of Coherence Scattering Domains (CSD) of HAP in Samples Obtained by the CPS- and PPS-Reactions[a]

	CPS reaction					PPS reaction	
	along [001]		along [100]			along [001]	
initial gelatin content [g]	fwhm of (002)- reflection	length of CSD [nm]	fwhm of (300)-reflection	length of CSD [nm]	aspect ratio c/a	fwhm of (002)-reflection	length of CSD [nm]
0	0.532	23.5	1.743	7.5	3.1	0.359	34.9
9	0.546	22.9	1.903	6.8	3.3	0.389	31.5
30	0.568	22.1	2.002	6.5	3.4	0.425	29.5
50	0.512	24.5	2.311	5.6	4.3	0.428	29.3

[a] Calculations are performed by the use of the Scherrer equation;[48] X-ray powder patterns are shown in Figures 2 and 3.

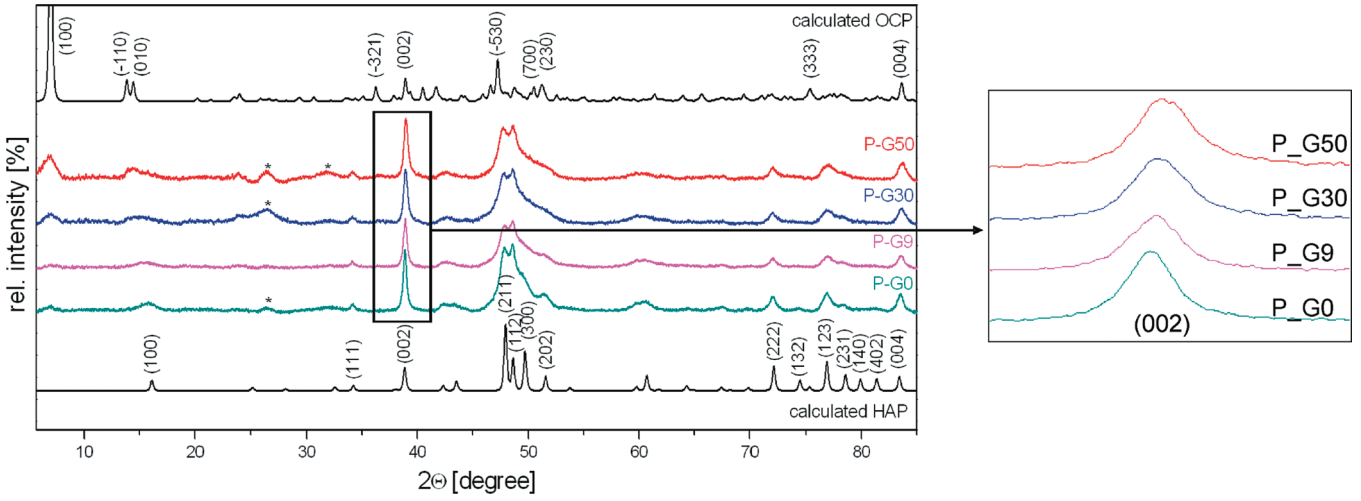

Figure 3. XRD patterns ($CrK_{\alpha 1}$) of samples precipitated by the PPS reaction and gelatin amounts of 0 g, 9 g, 30 g, and 50 g (P-G0, P-G9, P-G30, and P-G50) together with the calculated powder patterns of OCP[49] and HAP.[50] The broadness of the (002) reflections increases with increasing gelatin concentration. Reflections marked with an asterisk belong to vaseline as well as to poorly crystalline calcium phosphates. For further details see the text and Figure 2b.

XRD patterns ($20° < 2\theta < 33.5°$) of vaseline and reaction products with and without vaseline. Thus, the reflections appearing at ~26° and ~32° not only belong to vaseline but also to the poorly crystalline parts (or even ACP) increasing with increasing gelatin contents. In order to determine the influence of gelatin on the size of the HAP nanosubunits (coherence scattering domains, CSD) along the *a*- and *c*-axes, the peak broadenings of the (300)- and (002)-reflections of HAP were used. The results of the calculations using the Scherrer equation[48] are presented in Table 1, showing that for samples prepared with initial gelatin contents from 0 to 50 g the length of the CSDs along [100] monotonically decreases. In contrast, the length of CSDs along [001] is not significantly affected by the initial concentration of gelatin and remains almost the same (22−25 nm). Thus, with increasing gelatin content the HAP nanosubunits become more elongated compared with the less anisotropic (less elongated) habit of HAP prepared without gelatin. This trend in particle size and habit was also observed by Chang et al.[19−22]

The XRD patterns of samples precipitated by the PPS reaction and gelatin amounts of 0 g, 9 g, 30 g, and 50 g (P-G0, P-G9, P-G30, and P-G50) are represented in Figure 3 (in addition, the calculated powder patterns of HAP[50] and OCP[49] are given). The results show that samples prepared by the PPS reaction contain a mixture of HAP and OCP. Because of the structural similarity between OCP and HAP,[49] most of the reflections in the XRD patterns are overlapping; thus, it is difficult to allocate the corresponding reflections in the experimental patterns. However, the diffraction peak at $2\theta \approx 7°$ ($CrK_{\alpha 1}$-radiation) is characteristic for OCP (d_{100} = 18.6 Å), whereas that at $2\theta \approx 16°$ is characteristic for HAP (d_{100} = 8.1 Å). Thus, they can be used as diagnostic reflections for the presence of OCP and HAP in the products. As illustrated in Figure 3, the content of OCP in the materials increases with increasing initial concentration of gelatin. However, just from XRD it is difficult to prove whether the sample synthesized with the highest amount of gelatin (P-G50) exclusively contains OCP. Earlier, Iijima et al.[52] demonstrated that the formation of HAP and OCP strongly depends on the initial Ca/P ratio in the solutions. OCP is preferentially precipitated from a solution with a small Ca/P ratio, while apatite is formed at higher Ca/P ratios. This can be the reason why in our experiments OCP is observed in the samples precipitated by the PPS reaction and not in the samples obtained by the CPS mode. Furthermore, gelatin can prevent or inhibit the further phase transformation of OCP to HAP.[53] In general, the apparently more narrow and resolved peaks in

(52) Iijima, M.; Kamemizu, H.; Wakamatsu, N.; Goto, T.; Doi, Y.; Moriwaki, Y. *J. Cryst. Growth* **1991**, *112*, 467.
(53) Bigi, A.; Boanini, E.; Cojazzi, G.; Falini, G.; Panzavolta, S. *Cryst. Growth Des.* **2001**, *1*(3), 239.

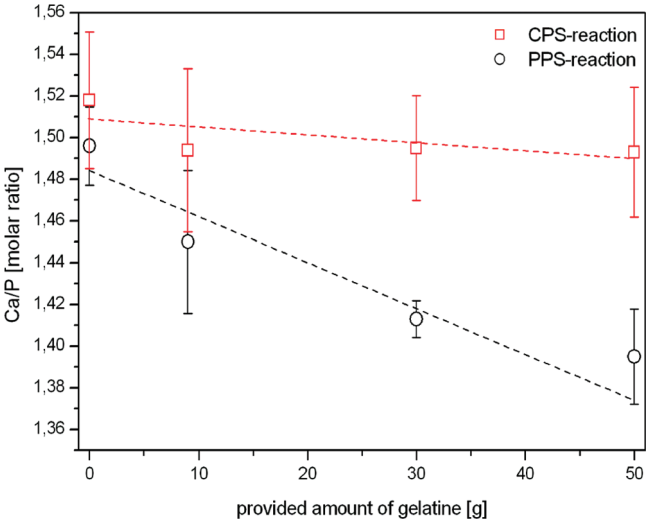

Figure 4. Molar ratios Ca/P of the composites determined by EDX analyses. The error bars represent the standard deviations of six to nine independent determinations. The dashed lines correlate with the partial regression lines. For further details, see the text.

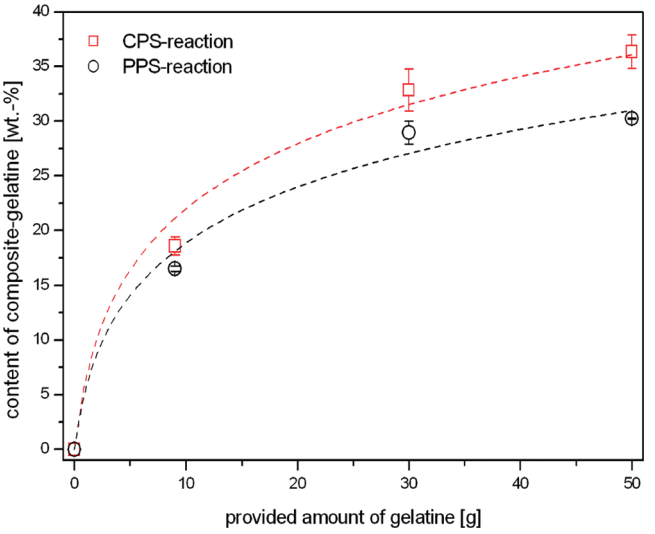

Figure 5. Gelatin content of the composites. The error bars represent the standard deviations of six to nine independent determinations. The dashed lines correlate with the partial regression lines. For further details, see the text.

the XRD patterns can be attributed to a better crystallinity of the PPS samples compared to that of samples precipitated by the CPS reaction. In addition, the relative intensities of the reflections at 2θ around 26° and 32° (peaks marked with an asterisk, Figure 3) are significantly smaller compared with the respective peaks in the in the XRD patterns of samples obtained by the Ca prestructuring reaction (Figure 2). The intensities of these peaks also increase with increasing gelatin content, probably indicating an increasing content of only poorly crystalline or amorphous phases. The lengths of the CSDs of HAP (precipitated without gelatin, P-G0) along [100] and [001] amount to 7.5 and 34.9 nm, respectively. The broadness of the (002) reflections in the XRD patterns also increases with increasing gelatin concentration (Figure 3 and Table 1), which can be ascribed to either a decrease of the lengths of the CSDs or a result of overlapping reflections of HAP and OCP.

Chemical Composition. With respect to their ideal chemical formulas, hydroxyapatite ($Ca_5(PO_4)_3(OH)$) and octacalcium phosphate ($Ca_8(PO_4)_4(HPO_4)_2 \cdot 5H_2O$) are characterized by the molar ratios Ca/P = 1.67 and Ca/P = 1.33, respectively. The molar ratios Ca/P of the composites prepared by precipitation reactions in the presence of different amounts of gelatin (0 g, 9 g, 30 g, and 50 g) were determined by EDX analyses. The results for both, the CPS and the PPS reactions, are summarized in Figure 4. The data symbols represent average values from six to nine independent determinations. The Ca/P ratios of the composites obtained by the PPS reaction strongly depend on the amount of gelatin in the reaction mixtures: the Ca/P ratio decreases with increasing amount of gelatin in the reaction mixture. In case of the CPS mode, the Ca/P ratios remain nearly constant within the limits of error.

As already discussed in the X-ray diffraction section, the inorganic components of the composites consist of HAP + ACP and HAP + OCP + ACP, depending on the mode of precipitation (CPS and PPS routes, respectively). This observation is clearly reflected by the chemical bulk-compositions with the lower Ca/P ratios for the composites obtained by the PPS reactions.

The gelatin content in the composites was calculated on the basis of the analytical data obtained for the nitrogen content in the composites and in pure gelatin (pure gelatin contains 16.52 ± 0.19 wt % nitrogen). Nitrogen was used as the reference element instead of carbon because of the presence of carbonate in the apatite component of the composites, as shown by the FT-IR investigations. Independent of the prestructuring ion in the solutions, the content of the composite gelatin increases exponentially (see Figure 5). The samples obtained by the CPS reaction contain slightly more gelatin than those prepared by the PPS route.

The presence of $[PO_4]^{3-}$, $[HPO_4]^{2-}$, $[OH]^-$, $[CO_3]^{2-}$, and H_2O (inorganic phases: HAP[3,54,55] OCP[56]) as well as protein molecules[57] within the precipitated components were monitored by FTIR-spectroscopy. The FT-IR spectra of samples precipitated by the CPS reaction method exhibit the four modes (ν_1, ν_2, ν_3, and ν_4) of the internal vibration of the phosphate group corresponding to the apatite crystal structure. The ν_1 band appears at 960 cm^{-1}, ν_2 at 468 cm^{-1}, ν_3 in the region from 1030 cm^{-1} to 1100 cm^{-1}, and ν_4 at 565–603 cm^{-1}. In addition, infrared adsorption bands of carbonate were found at 876 cm^{-1} (ν_2), 1424 cm^{-1}, and 1460 cm^{-1}(ν_3) corresponding to the B-type carbonate substitution (phosphate replacement).[43] The bands corresponding to the $[HPO_4]^{2-}$ group are detected as broad shoulders at about 550 cm^{-1} and 865 cm^{-1}. A broad band in the high energy region from 3700 cm^{-1} to 2700 cm^{-1} and a band at about 1645 cm^{-1} can be assigned to the water molecule's stretching and bending modes, respectively. $[OH]^-$ groups (located inside the channels) of the apatite component of the composite are indicated by a broad band at 640 cm^{-1} and a weak

(54) Dorozhkin, S. V. *J. Mater. Sci.* **2007**, *42*, 1061.
(55) Rey, C.; Shimizu, M.; Collins, B.; Glimcher, M. J. *Calcif. Tissue Int.* **1990**, *46*, 384.
(56) Fowler, B. O.; Markovic, M.; Brown, W. E. *Chem. Mater.* **1993**, *14*, 937.
(57) Doyle, B. B.; Bendit, E. G.; Blout, E. R. *Biopolymers* **1975**, *14*, 937.

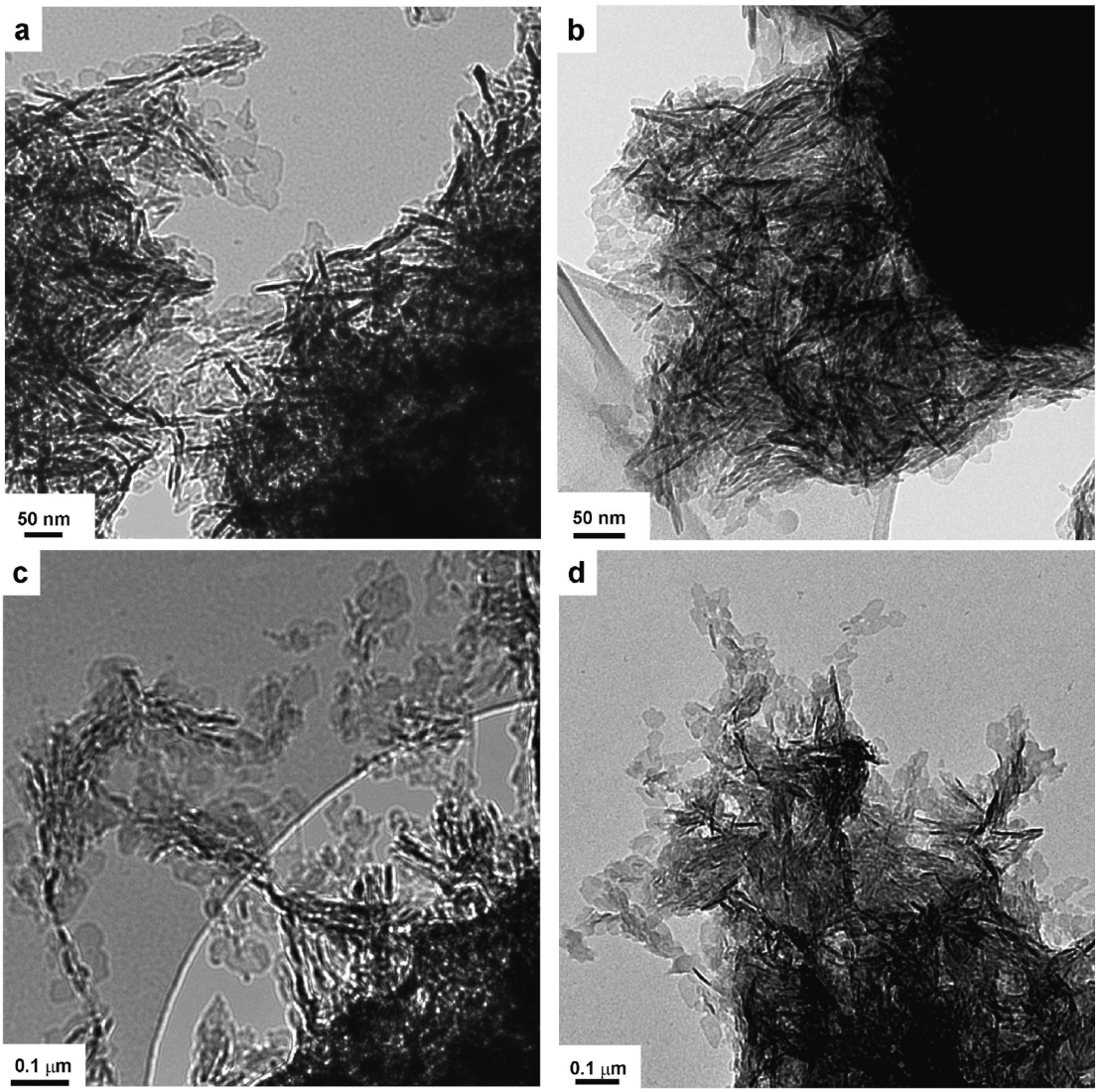

Figure 6. C-TEM images of samples precipitated by means of the CPS reaction using various amounts of gelatin (a, 0 g of gelatin, C-G0; b, 9 g of gelatin, C-G9; c, 30 g of gelatin, C-G30; d, 50 g of gelatin, C-G50). The particles preferably form large agglomerates surrounded by flat laying plates with an average size of 50 nm × 33 nm. The agglomerate's interior seems to consist of needles which, however, are present as plates in an orientation perpendicular to the incident electron beam (see Figure 7).

(but very sharp) band at 3570 cm^{-1}, which can be assigned to vibrational and stretching modes, respectively. Furthermore, the FT-IR spectra of the samples obtained in the presence of gelatin (C-G9, C-G30, and C-G50) exhibit bands at 1660 cm^{-1}, 1546 cm^{-1}, and 1240 cm^{-1}, which can be assigned to the gelatin components amide I, amide II, and amide III, respectively. Additionally, amide A and B exhibit bands at 3070−3300 cm^{-1}, which overlap with the stretching modes of the water molecules. The vibration modes of the CH groups of the gelatin molecules were found at 2853 cm^{-1}, 2925 cm^{-1}, and 2960 cm^{-1}. The relative intensities of the FTIR bands attributed to the gelatin molecules increase with increasing content of gelatin in the precipitated materials.

The FT-IR spectra of samples obtained by the PPS reaction without gelatin (P-G0) are similar to that of the sample precipitated by the CPS mode (C-G0). However, with increasing gelatin content (P-G9, P-G30, and P-G50), the spectra of samples synthesized by the PO_4 prestructuring reaction show additional bands at 870 cm^{-1}, 915 cm^{-1}, 1206 cm^{-1}, and 1290 cm^{-1} which can be ascribed to $[HPO_4]^{2-}$ groups present in the OCP crystal structure. The relative intensities of these bands, as well as of the bands corresponding to gelatin molecules, increase with increasing gelatin content of the composite materials.

Particles Morphology and Structure. Conventional TEM (C-TEM) was used in order to reveal the morphology (shape, size, and agglomeration behavior) of the precipitated composites. Particle thicknesses were determined by electron holography. Crystalline phases of the inorganic part of the composites and the presence of gelatin were investigated by high resolution TEM (HR-TEM) and electron diffraction.

Figure 6 illustrates the C-TEM images of samples precipitated by the CPS reaction method and gelatin amounts of 0 g, 9 g, 30 g, and 50 g (a, C-G0; b, C-G9; c, C-G30; d, C-G50). The images show large agglomerates

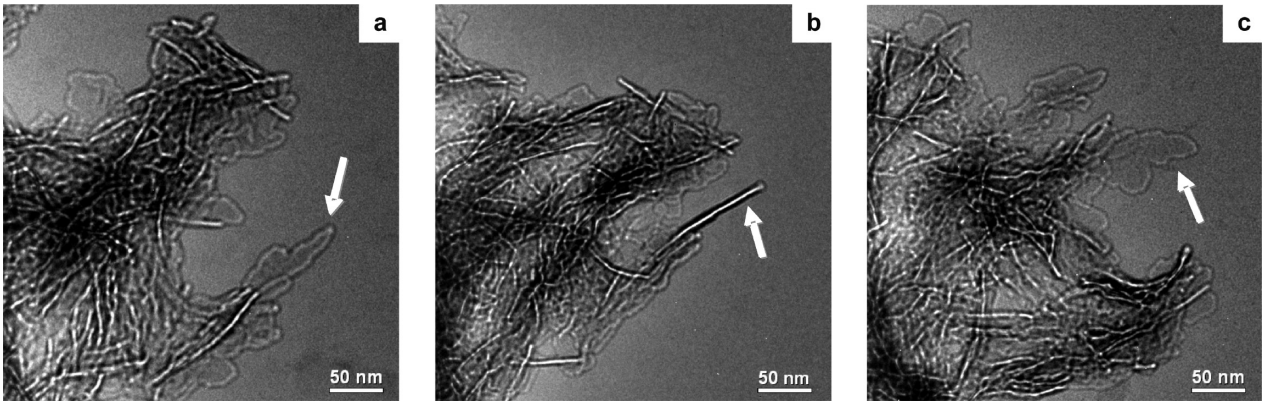

Figure 7. Tilting series (TEM) of a sample prepared by the CPS reaction with 30 g of gelatin (C-G30). (a) Sample situated at an angle of −50° with respect to the incident electron beam, (b) at −14°, and (c) at +46°. The series clearly illustrates that the needle-like particles in fact are small plates when tilted in an appropriate position perpendicular to the incident electron beam. The particle marked with a white arrow shows the bivalent plate-like−needle-like behavior.

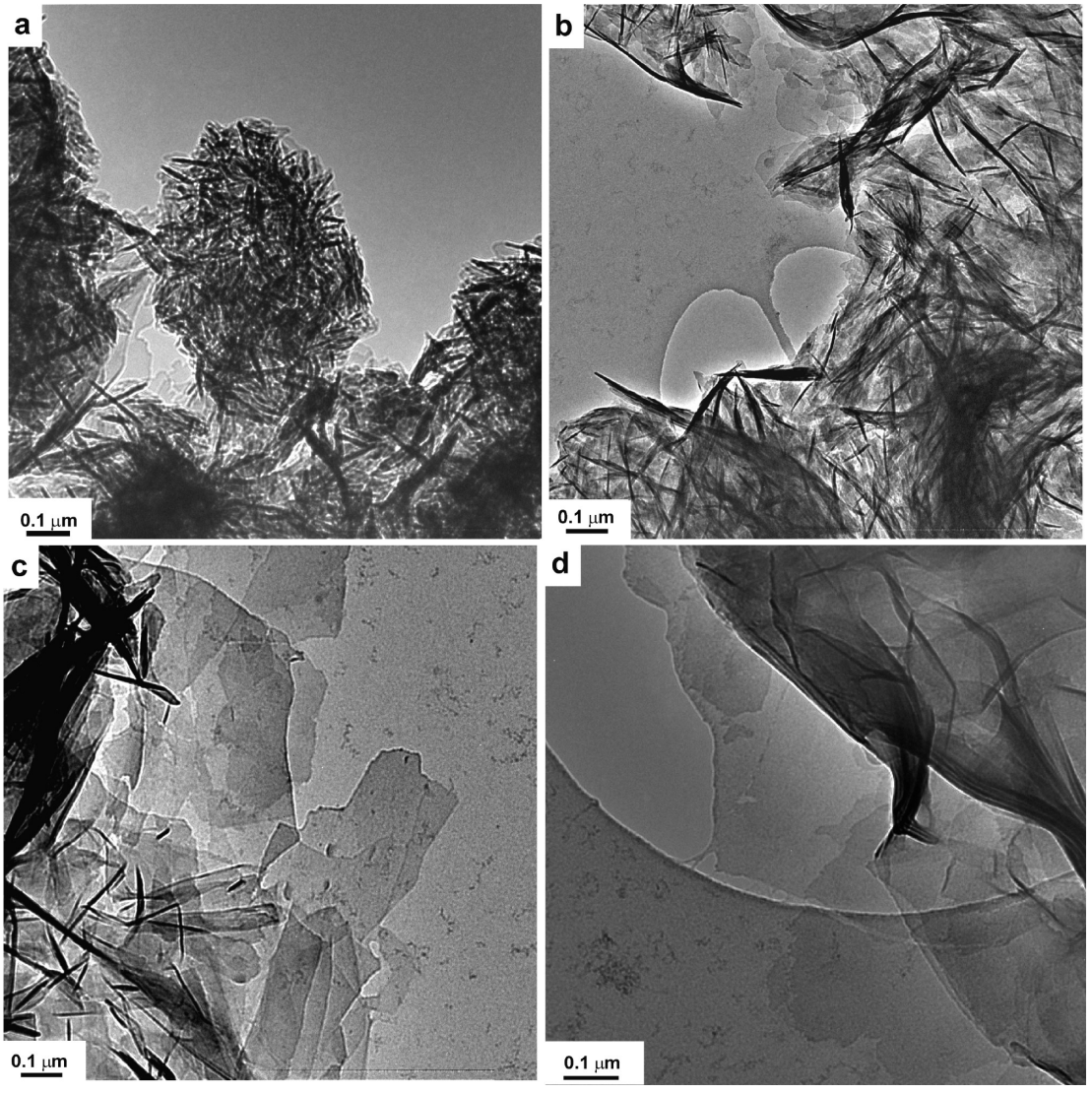

Figure 8. C-TEM images of samples precipitated by means of the PPS reaction with different amounts of gelatin. (a) 0 g of gelatin (P-G0), aggregates of small plates which are partially curled; (b) 9 g of gelatin (P-G9), aggregates of larger curled plates; (c) 30 g of gelatin (P-G30), aggregates of partly curled foils; (d) 50 g of gelatin (P-G50), large, partly waved foils. The particle size increases with rising amounts of provided gelatin.

of several hundred nanometers to several micrometers extension which are composed of smaller particles. Single, plate-like particles can be seen at the borders in the vicinity of the agglomerates with an average size of

50 nm × 33 nm independent of the provided amount of gelatin. The agglomerates seem to be composed of smaller needles with the same size as the surrounding plate-like particles. Such types of needle-like structures are mostly presented and described in the literature as the typical morphology of nano-HAP particles.[20−24,28,29]

However, the needle-like particles are actually not needles but small plates in an orientation upright on their edges normal to the surface. Thus, the impression of needles is evoked by the mass−thickness contrast in the TEM. Figure 7 represents TEM investigations performed by tilting the sample, thereby excluding the existence of needles. The sample (C-G30) was tilted at different angles and orientations of −50°, −14°, and +46° with respect to the incident electron beam. The particle marked with a white arrow indicates the bivalent plate-like−needle-like behavior by turning from a needle into a plate by tilting and vice versa.

Figure 8 displays C-TEM images of samples precipitated by the PPS reaction and offered gelatin amounts of 0 g, 9 g, 30 g, and 50 g (a, P-G0; b, P-G9; c, P-G30; d, P-G50). The particles are also arranged as agglomerates. The size of the precipitated particles is increasing with rising amounts of gelatin provided in the reaction. This observation is different in comparison with that with the CPS samples, in which the particle size is nearly unaffected by the amount of gelatin used for their preparation. The increase of the particle size with rising amounts of gelatin is plotted in Figure 9. For comparison, the particle sizes of the CPS samples are shown as well. In the absence of gelatin, the samples prepared by the PPS reaction (Figure 8a, P-G0) show a similar appearance compared with the CPS samples. They also reveal a needle-like morphology and are arranged to form agglomerates. Only a few particles at the brinks of the agglomerates are visible as small plates. The needle-like particles are actually also small plates with an average size of 60 nm × 35 nm (only their thin edges are visible or they are partially curled, a phenomenon typical for PPS-samples). Figure 8b (9 g of gelatin, P-G9) shows aggregates of middle sized, curled plates together with some flat laying species with an average size of 135 nm × 80 nm. Figure 8c (30 g of gelatin, P-G30) presents aggregates containing partly curled foils. The average particle size was determined as 460 nm × 340 nm. Samples prepared with 50 g of gelatin (P-G50, Figure 8d) also contain partly curled but very large foils with an average size of 730 nm × 410 nm.

The structure of the composite was investigated by HR-TEM. In Figure 10, TEM micrographs and the corresponding FFT of a sample precipitated by the CPS reaction (C-G30) are shown. The marked area in the overview image (Figure 10a) was examined in detail and is displayed as a zoomed image (Figure 10b) as well as a Bragg mask filtered image (Figure 10c). The interplanar distances of 8.1 Å and 3.4 Å for the (010) and (002) lattice planes of hexagonal HAP are labeled. Figure 10d presents the corresponding FFT along the [100] zone axis of the marked area in Figure 10b showing the interplanar distances of 8.1 Å and 3.4 Å. (0kl) and (0k-l) reflections are missing due to symmetry prohibition. The modulation

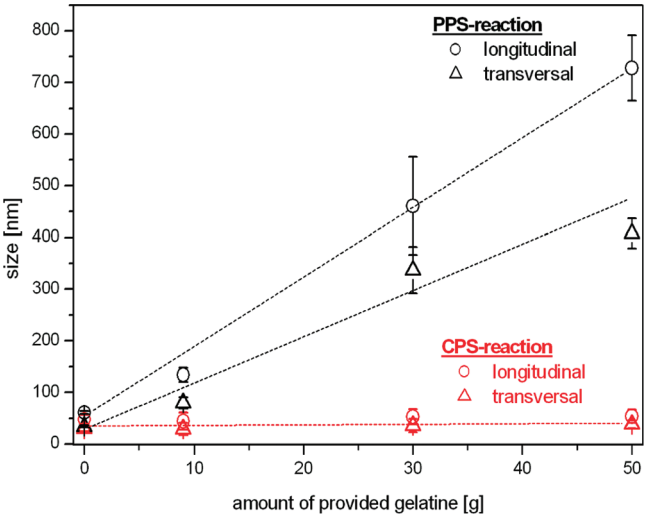

Figure 9. Particles sizes (C-TEM investigations) in longitudinal and transversal dimensions of samples prepared by means of CPS- and PPS reactions. Provided amounts of gelatin: 0 g, 9 g, 30 g, and 50 g (C-G0, C-G9, C-G30, C-G50, P-G0, P-G9, P-G30, and P-G50). The diagram shows that samples prepared by the CPS reaction do not significantly change their particle size dependent on the provided amount of gelatin, whereas samples prepared by the PPS reaction show a nearly linear increase of the particle size with rising gelatin amounts from 0 g to 50 g (for numerical values, see the text). Error bars represent the standard deviations of 10 to 15 particles. Dashed lines correlate with the partial regression lines.

within the HAP-pattern as shown in Figure 10c is assumed to be caused by intergrowth with the organic component (also see Figure 13).

Figure 11b presents the high resolution electron micrograph of a particle prepared by the PPS reaction (P-G30). The enlarged micrograph of the marked area in Figure 11a is given in Figure 11b. Figure 11c shows the magnified and filtered image of the marked area in Figure 11b. Figure 11d shows the corresponding fast Fourier transform (FFT) along the [100] zone axis of the marked area in Figure 11b. The interplanar distances of 9.1 Å and 3.3 Å correspond to the (010) and (002) lattice planes of OCP, respectively. The diffuse ring around the center beam indicates the amorphous parts of the material. The reflection intensities in general are very weak due to the low crystallinity of the sample and due to the low particle thickness of only a few unit cells. The areas 1 and 2 in Figure 11c represent separate crystalline domains within the sample. The interface between the domains appear as more diffuse parts and are assumed to consist of gelatin and/or amorphous calcium phosphate.

Particle thicknesses of the samples were determined by means of electron holography. For this, the inner potential U_i of the inorganic component of the nanocomposites was calculated to be 16.6 V for HAP and 12.9 V for OCP.[58] For gelatin, the inner potential U_i was chosen as 8.5 V, a value corresponding to polystyrene.[59] The inner potential U_i* of the composite material was calculated on the basis of the relative amounts of gelatin and the

(58) Voelkl, E.; Allard, L. F.; Joy, D. C. *Introduction to Electron Holography*; Kluwer Academic/Plenum: New York, 1999.
(59) Wang, Y. C.; Chou, T. M.; Libera, M.; Voelkl, E.; Frost, B. G. *Microsc. Microanal.* **1998**, *4*, 146.

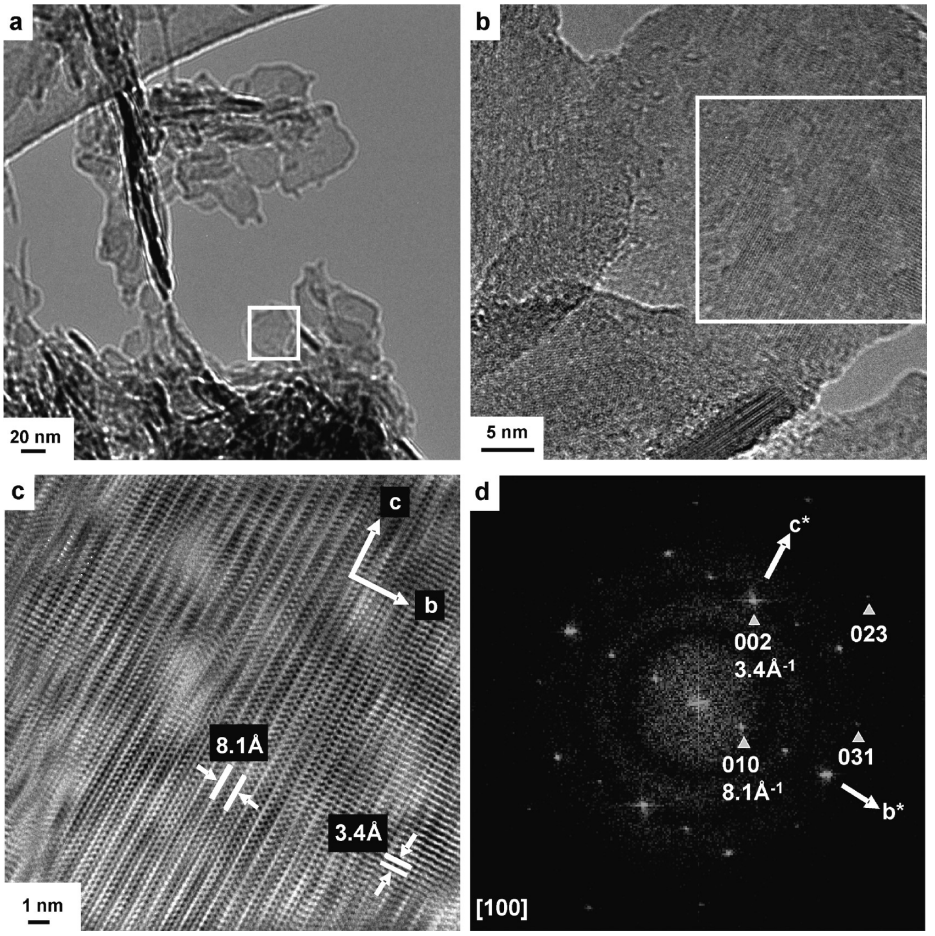

Figure 10. (a) C-TEM image of a composite sample prepared by the CPS reaction (C-G30); (b) HR-TEM image of the marked area in panel a; (c) enhanced and filtered (Bragg mask) image of the marked area in panel b; (d) the corresponding FFT along the [100] zone of the marked area in panel b. The interplanar distances of 8.1 Å (010) and 3.4 Å (002) indicate the presence of HAP as the inorganic component of the composite.

inorganic component. The gelatin amount was determined by chemical analysis (see Figure 5), and the missing fraction to 100% was ascertained as the inorganic component. When calculating U_i* for samples prepared by the CPS reaction, HAP was taken as the inorganic component. For samples prepared by the PPS route, without or in the presence of 9 g of gelatin, HAP was supposed as the inorganic component, whereas for samples with 30 or 50 g of gelatin, OCP was taken as the mineral part. The resulting inner potentials U_i* are given in Table 2.

Figure 12a shows the reconstructed phase image of an electron hologram of a sample prepared by the CPS reaction (C-G30). Figure 12b presents the resulting height profile of the region marked in Figure 12a. Two steps can be recognized with a first phase shift of 0.5 rad and a second phase shift of 0.3 rad. The phase shift of 0.5 rad is in accordance with a thickness of 4.9 nm, whereas the second phase shift of 0.3 rad corresponds to 2.9 nm. Figure 12c illustrates the corresponding 3D-structure plot of the reconstructed phase image shown in Figure 12a. The color code indicates the difference of a phase shift of 0.2 rad between blue, green, red, and yellow.

Representative values for the thickness of particles of samples either prepared by CPS or PPS reactions were already given in Table 2 (calculations from X-ray powder patterns by use of the Scherrer equation[48]). The TEM investigations (Figures 10 and 11) revealed that the crystallographic directions perpendicular to the plane faces correspond to [100] in the case of HAP and to [110] for OCP. The thickness determinations on separate particles by the use of electron holography clearly reveal that they often consist of stacks of thin plates. It is not clear at present whether the thin plates (with a thickness down to ~3 nm) are grown together or just lie on top of each other. The latter scenario would allow a lattice mismatch, which could be one of the reasons for the poor quality of the FFT patterns (together with a mosaic structure on the nanoscale within each plate).

The first results revealing the inner structure and thus the ordering of the organic component within the nanocomposites are shown in Figure 13. After treatment of the particles with 0.2 N EDTA(aq) (partial dissolution of the inorganic component) followed by staining with UAc(aq), gelatin fibrils are clearly observed in a more or less parallel arrangement (Figure 13a). The diameter of a single fibril is about 4 nm. The fibrils are best ordered close to the borders of the composite particles and preferably extend parallel to their plane faces. The electron diffraction of Figure 13b (see inset) shows gelatin fibrils running parallel to the *c*-axis of HAP particles.

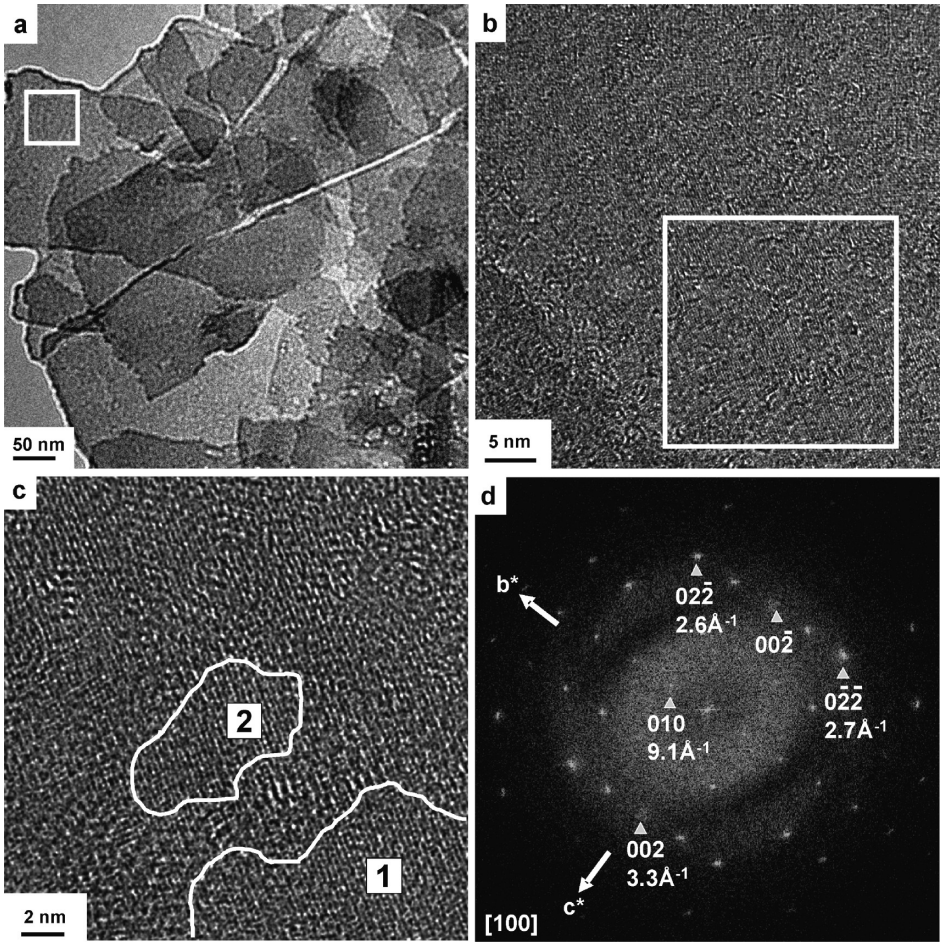

Figure 11. (a) C-TEM image of a composite sample prepared by means of the PPS reaction (P-G30); (b) smoothed HR-TEM image of the marked area in panel a; (c) enhanced image of the marked area in panel b; (d) corresponding FFT of the marked, but unsmoothed area in panel b along the [100] zone. Interplanar distances of 9.1 Å (010) and 3.3 Å (002) indicate the presence of OCP. The two numbered areas in panel c illustrate the mosaic-arrangement of separated domains. The diffuse parts between and around areas 1 and 2 are assumed to consist of gelatin or amorphous calcium phosphates.

Table 2. TEM Investigations of the Composites: Size, Inner Potential (U_i*), and Thickness (Determined by Electron Holography) of Precipitated Particles Prepared by the CPS- and PPS-Modes

	CPS reaction			PPS reaction		
provided amount of gelatin [g]	size [nm]	U_i*	thickness [nm]	size [nm]	U_i*	thickness [nm]
0	48 × 30	16.6	4−10	60 × 35	16.6	2−5
9	45 × 30	15.1	3−8	135 × 80	15.2	3−5
30	53 × 36	13.9	3−9	460 × 340	11.6	4−7
50	54 × 38	13.7	5−13	730 × 410	11.6	6−8

Application as Dentine Repair Material. The nanocomposite prepared by the CPS reaction (C-G30) shows a relatively good agreement with human dentine (C-G30/human dentine; Ca/P, 1.50/1.61; total organic, 33/20 wt %). A material related to C-G30 was already proven to have a beneficial effect on the occlusion of dentine tubules.[41,60−63] Such properties are of special interest for the treatment of sensitive teeth because 45% of Europeans and 37% of Northern Americans suffer from this problem.[64] According to ref. 41, the nanosized hydroxyapatite/gelatin composite together with human saliva act as a neomineralizing agent on dentine.

On the basis of these observations, we investigated an OCP/gelatin composite (P-G30) in order to find out whether this material shows an effect of neomineralization on dentine slabs similar to that shown by HAP/gelatin composites. The preparation of dentine slabs as well as the mode of treatment with the composite was already described in the Experimental Section. The results evidenced that the composite P-G30 is also suitable to act as a neomineralizing agent on dentine. Figure 14 represents a bovine dentine slab before and after treatment with a 2 wt % dispersion of P-G30 in water/glycerine (1:3). Even though this material consists of a mixture of OCP and HAP as the inorganic component and not exclusively of HAP (as dentine does), our investigations show a very good effect with respect to the occlusion of the tubules. It can be stated that the composite

(60) Schroeder, H. E. *Orale Strukturbiologie*, 4th ed.; Georg Thieme Verlag: Stuttgart, Germany, 1992.
(61) Daculsi, G.; Menanteau, J.; Kerebel, L. M. *Calcif. Tissue Int.* **1984**, *36*, 550.
(62) Braunbarth, C.; Franke, H.; Poth, T.; Schechner, G.; Kniep, R.; Kropf, C.; Wülknitz, P. VDI-Reports No. 1803, **2003**.
(63) Kniep, R.; Bordas, A.; Braunbarth, C.; Franke, H.; Poth, T.; Schechner, G.; Kremer, J.; Kropf, C.; Wülknitz, P. *J. Dent. Res.*, **2004**, *83* (Special Issue A).
(64) Graham, F. L.; Tatton-Brown, C.; Meert, G.; Alexander, D. C. *J. Dent. Res.* **2003**, *82*, B134.

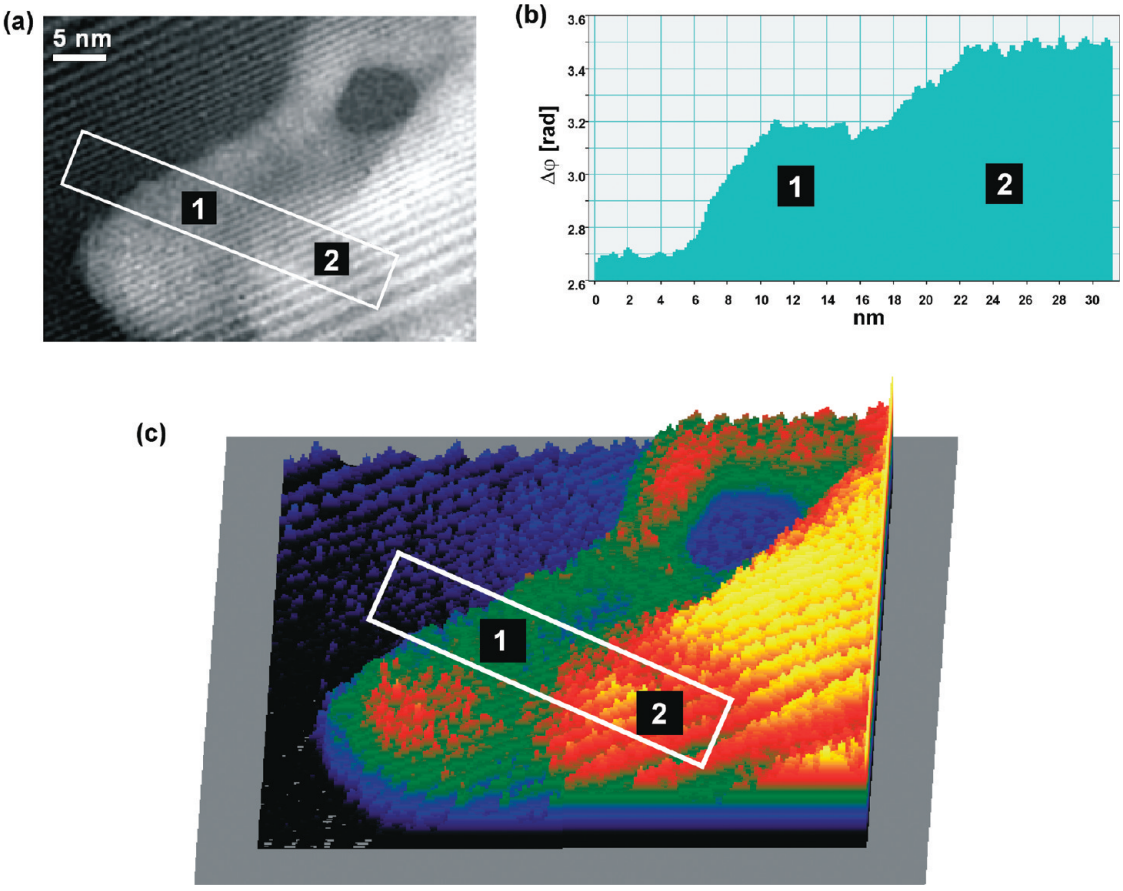

Figure 12. (a) Reconstructed phase image of an electron hologram of a particle of a sample prepared by means of the CPS reaction (C-G30). The bright area represents the sample, whereas the dark area corresponds to a vacuum. Area 1 represents a first plate, and area 2 indicates a second plate on top of the first one. The topography is visualized by the corresponding height profile. (b) Height profile of the marked area in panel a. The steps indicate the phase shift between the vacuum and area 1 (0.5 rad indicating a foil thickness of 4.9 nm), and the phase shift between area 1 and area 2 (0.3 rad representing a foil thickness of 2.9 nm). (c) Corresponding 3D-plot of the reconstructed phase image from panel a. The color code indicates a phase shift of 0.2 rad among blue, green, red, and yellow.

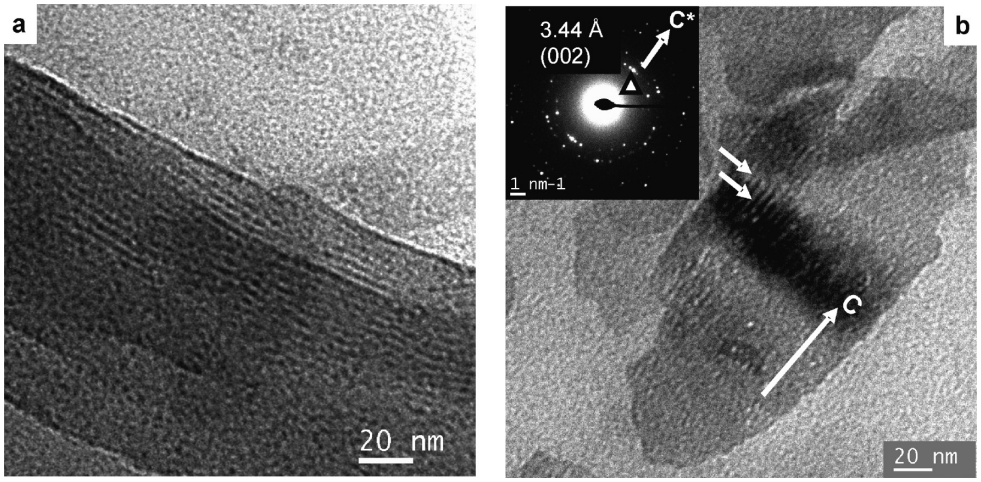

Figure 13. (a) TEM micrograph showing the arrangement of gelatin fibrils within a composite plate. The sample (CPS reaction; C-G30) was treated with 0.2N EDTA(aq) followed by staining with 0.5 wt.% UAc(aq). (b) The c-axis of HAP-crystals is running parallel to the gelatin fibrils (marked with short white arrows). For further details, see the text.

dispersion acts as a nucleating agent for neomineralization processes with the gelatin increasing this effect and taking the function of a natural glue between dentine and the growing layer.

Even more pronounced is the effect of neomineralization (formation of a protection layer on bovine dentine) by the use of the composite C-G30 as the active component in a conventional tooth paste (see Experimental Section). The results of our detailed FIB and TEM investigations are summarized in Figure 15. The mode of FIB preparation of a thin slab consisting of the dentine part (together with the tubules) and the artificial

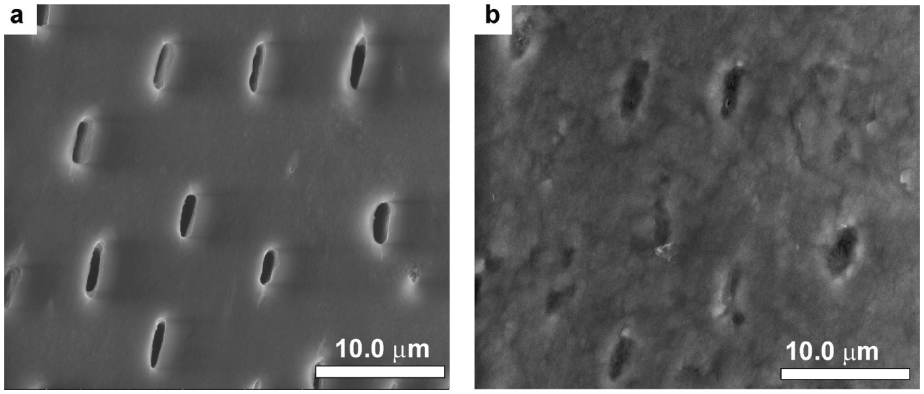

Figure 14. ESEM images of bovine dentine slabs. (a) Before treatment and (b) after treatment with a 2 wt % dispersion of P-G30 in water/glycerine (1:3). The treatment leads to occlusion of the tubules.

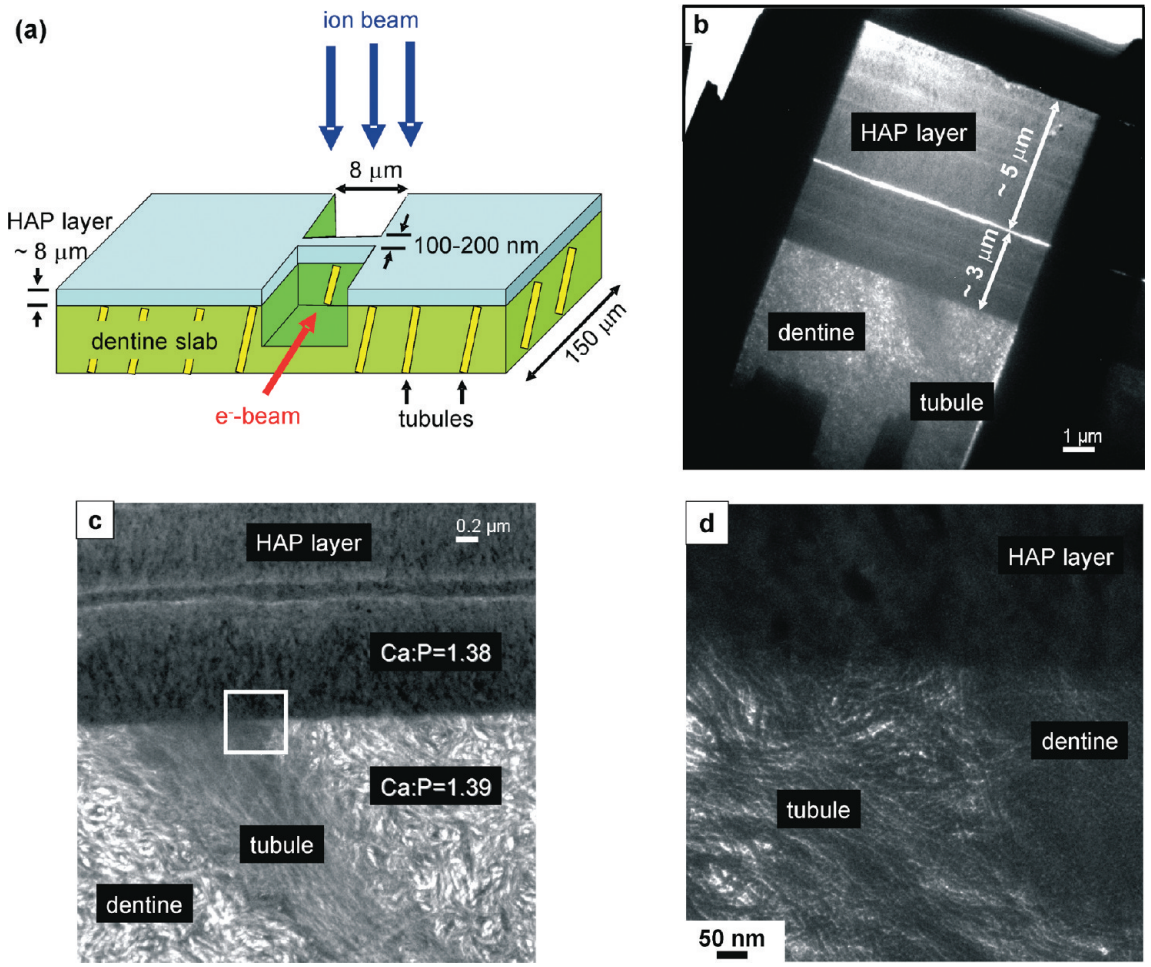

Figure 15. (a) FIB sample preparation of a dentine bovine slab covered with an artificial on-grown HAP−gelatin composite protection layer. First, the slab is thinned in cross-section with a window size of about 8 μm. Subsequently, the resulting lamella (thickness 100 nm−200 nm) is laterally separated from the bulk in order to release stress. (b) TEM micrograph (overview) of a cross-sectional FIB thin cut of the dentine slab. The on-grown apatite−gelatin composite protection layer appears dark due to the higher content of inorganic material compared with dentine. The total thickness of the on-grown layer amounts to 8 μm and is composed of individual layers which are formed by the treatment procedure (morning/afternoon-brushing). The horizontal crack (white line) might be caused by internal stress during FIB preparation. (c) Dentine substrate with a tubule (bottom) and the on-grown HAP−gelatin composite protection layer (top) at higher magnification. Ca/P ratios (EDX-analyses) of dentine and the protection layer are nearly identical. (d) Zoomed image of the marked area in panel c. Interface dentine/protection layer without indications for weakening effects and poor intergrowth.

(up-grown) layer is shown in Figure 15a. Within a 10 day period (repeated brushing and neomineralization in an artificial salvia solution), a layer of 8 μm thickness was grown on the top of the dentine slab (Figure 15b). EDX analyses reveal nearly identical ratios of Ca/P for dentine and the protection layer. Because of the higher amount of the crystalline (inorganic) phase in the protection layer, this artificial area appears more dark in the TEM images (Figure 15c). The horizontal stripes in Figure 15b and c are assumed to be caused by the different steps during the

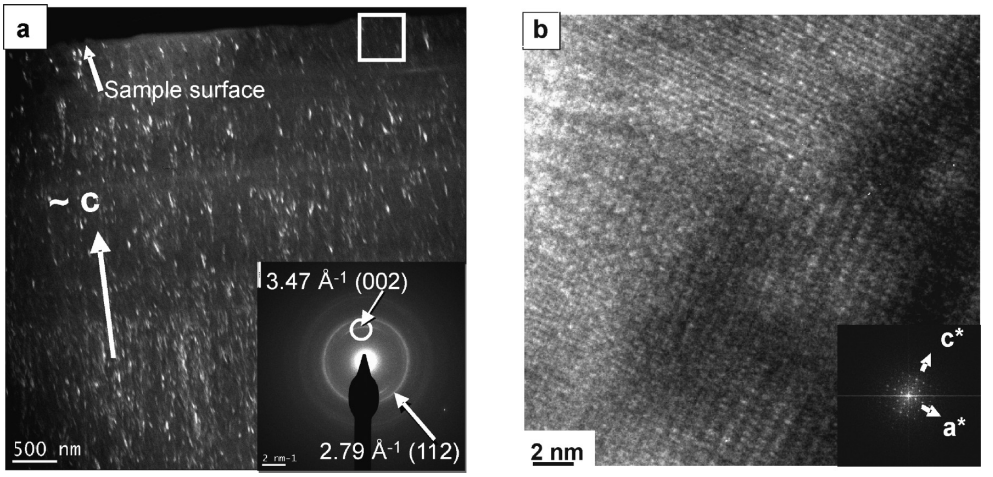

Figure 16. (a) TEM dark-field image of the artificial HAP−gelatin composite protection layer grown on dentine (Figure 15). For dark-field imaging, the enclosed area of the (002) reflection arch of apatite (see the inset) was chosen. Thus, only HAP crystallites oriented within the circle area (with a radius equivalent to 0.2°) are illuminated and appear bright. The (002) 2θ-value is about 0.6° for 100 kV (λ = 3.7 pm). The *c*-axes of HAP crystallites run more or less parallel and perpendicular to the surface of the on-grown layer. This situation reminds us of the structure of enamel. (b) HR-TEM of the on-grown layer (marked area in panel a) showing the basal [010] zone of HAP.

treatment procedure (brushing/salvia) and are caused by a higher amount of gelatin. The thick white horizontal line in Figure 15b represents a crack which was generated by an internal inner stress caused by the FIB preparation. The interface dentine/protection layer is sharp, and the tubule is perfectly closed. This interface is also stable during FIB preparation and is not affected by the brushing procedures. No indications concerning any areas of low stability within the interface have been obtained in the course of our investigations. Figure 15d shows the enhanced image of Figure 15c. The dark-field pattern of the protection layer imaged by the (002) reflection of HAP clearly reveals that the crystalline subunits are elongated and arranged more or less parallel in a direction perpendicular to the surface of the artificial layer (see Figure 16a). This structural (and compositional) situation is closely related to that of biogenic enamel.[54] The HR-TEM of the protection layer is shown in Figure 16b and represents the pattern of HAP.

Conclusions

A preparation strategy is described which allows the preparation of larger amounts of nanosized calcium phosphate−gelatin composites with constant (reproducible) properties. Depending on the mode of preparation (Ca-prestructuring/phosphate-prestructuring/amount of gelatin provided), the composite is well-defined with respect to particle size, phase composition, and the amount of gelatin included. In general, the composite particles are obtained as plates with dimensions ranging from 30 nm × 60 nm (CPS mode; inorganic phase, ACP and ACP + HAP, respectively) to about 400 nm × 700 nm (PPS mode; inorganic phase, OCP). The platy composite particles are characterized by intrinsic domains and mosaic structures with the crystallographic directions [100] for HAP and [110] for OCP running perpendicular to the plane faces.

As shown for a composite obtained by the CPS route, the gelatin included is present as microfibrils (~4 nm in diameter) preferably running parallel to each other and extending within the plates (parallel to the *c*-axis of HAP). Investigations by electron holography revealed the lowest steps on the particle plates going down to ~3 nm in height, which means that even very thin composite plates might be prepared, in which case a large-foil character should be clearly affected by tendencies of coiling. Weak coiling effects are already observed for the biggest composite plates (400 nm × 700 nm) obtained by the PPS route.

One of the motivations for the present work was to investigate the different prestructuring reactions (CPS and PPS) and their effects on the reaction products. The basic idea behind the work was our recent observation of stiffening of gelatin by calcium complexation within the triple-helical gelatin molecules and keeping their flexibility by outside phosphate attachment via hydrogen bonds.[39−44] In case of applying the double-diffusion technique, the different modes of pretreatment of gelatin led to the fan-like morphogenesis (Ca-prestructuring) and to the fractal morphogenesis (PO_4-prestructuring). By using the precipitation route, there are also clear differences in the shape development of the composites, but even the phase composition is different as described before (HAP (+ ACP) vs (HAP + ACP) + OCP). Concerning the shapes of the composite particles, the general differences between CPS and PPS modes can be given as follows: the CPS route leads to smaller sizes of the coherence scattering domains and to overall smaller particle sizes (nearly independent of the initial amount of gelatin); the PPS route leads to an increase of the size of the coherence scattering domains and the formation of large foils which are significantly smaller in thickness (dependent on the initial amount of gelatin). Altogether, the stiffening of gelatin by Ca-impregnation is assumed to cause higher ordering of the composite with respect to inorganic/organic structural correlations. In the case of PO_4 impregnation, the number of nucleation centers provided seems to be significantly enlarged leading to faster mineralization.

Chemical composition and structure (on the nano/mesoscale) of the composites closely resemble those of biogenic (human) hard tissues. In fact, the composites can be used as dentine repair materials as shown by in vitro experiments. The composites adhere onto dentine surfaces and act as seeds for neomineralization processes based on the supersaturation of saliva according to calcium and phosphate ions. By this, a protection layer of an apatite−gelatin composite with a structure closely related to biogenic (human) enamel is grown on the dentine surface, closing open tubuli, and, which in analogy to the biogenic material, is able to undergo processes of de- and remineralization.

Acknowledgment. We acknowledge the following staff members of the Max Planck Institute for Chemical Physics of Solids for experimental support and fruitful discussions: Dr. Raul Cardoso, Dr. Yurii Prots, Dr. Horst Borrmann, Dr. Gudrun Auffermann, and Professor Dr. Hannes Lichte (TU Dresden, Triebenberg Laboratory). We also would like to thank Dr. Daniel Wolf who provided the tilting series presented in Figure 7.